THE ASTROPHYSICAL JOURNAL, **262**:396–406, 1982 November 1

ON THE FLARING OF COMETARY PLASMA TAILS

ALEXANDER I. ERSHKOVICH,[1] MALCOLM B. NIEDNER, JR., AND JOHN C. BRANDT
Laboratory for Astronomy and Solar Physics, NASA Goddard Space Flight Center, Greenbelt, Maryland
Received 1982 January 11; accepted 1982 May 3

ABSTRACT

Wide-angle photographs of cometary plasma tails have been examined in connection with the large-scale shape of these tail systems, with specific emphasis on the flaring (or widening) of the tail with distance from the head. Photographs of comets Kohoutek 1973f and Bradfield 1974b taken at the Joint Observatory for Cometary Research show that on some days the flaring phenomenon is quite prominent, the tail subtending an angle of a few degrees, whereas on other days there is almost no flaring and the tail is cylindrical in shape.

On the assumption that hypersonic pressure balance with the solar wind governs the shape of plasma tails, it is found that the gas pressure of tail ions and the magnetic field strength at the flanks of the ionopause control the flaring state. The gas pressure exhibits the larger effect: for constant pressures above a certain critical value, the tail flares essentially without limit, whereas for smaller values the tail flares only near the head (becoming cylindrical at greater distances). The effect of the magnetic field is that the tail flares to larger distances the higher the field strength at the flanks of the ionopause. The observed variability in flaring (and the implied differences in gas pressure and magnetic field) are considered the result of changes in the position and shape of the Sunward cometary ionopause. Finally, insertion of reasonable comet and solar wind parameters into the pressure balance equations yields good agreement with the observations.

Subject headings: comets — hydromagnetics — interplanetary medium — plasmas

I. INTRODUCTION

The plasma tails of comets are tubes of magnetic flux captured from the interplanetary magnetic field and made observable in white light by fluorescing ions (primarily CO^+) spiraling from the head down along the field lines and into the tail (Alfvén 1957; see also Brandt and Mendis 1979). It is the *visibility* which distinguishes comet tails from other similar magnetic tail structures in the solar system (e.g., the magnetotails of Venus, Earth, and Jupiter), and which makes possible their use (from *remote* imaging) both as giant plasma physics laboratories and as natural probes of the solar wind. Moreover, the study of comet tails may have direct application to the general interaction of the solar wind with other intrinsically nonmagnetic bodies such as Venus, and vice versa; for a discussion of the analogies between Venus and comets in terms of their solar wind interactions, the reader is referred to Russell *et al.* (1982).

The magnetic fields thought to thread cometary plasma tails have never been observed directly as no spacecraft has yet visited a comet and the expected field strengths are too small to produce any spectroscopic effect (see Brandt 1968). Several lines of indirect evidence exist, however, concerning both the presence and the strength of the tail fields. First, the gyroradius of CO^+ ions obviously cannot exceed the visible radius of a tail ray (<3000 km), whence one obtains $B_T \geq 0.2$–0.8γ for CO^+ thermal energies in the range from 1 to 10 eV. Second, analysis of the helical wave motions sometimes seen far down the tails of bright comets yields an estimate of the tail field strength if one assumes that the waves are due to the Kelvin-Helmholtz instability; according to Ershkovich (1976, 1978, 1980), the field can exceed the ambient interplanetary field value by only about 50%. This estimate is in agreement with field strengths derived from pressure balance arguments (Ershkovich 1978, 1979, 1980).

Although much higher values for the tail field have been proposed in earlier papers using different approaches (e.g., Hyder, Brandt, and Roosen 1974; Ip and Mendis 1975, 1976; Mendis and Morrison 1979), it is noteworthy that the *Pioneer Venus* orbiter data have consistently yielded Venusian magnetotail field strengths of the order of 10γ, values not significantly in excess (if at all) of local interplanetary values. The *Pioneer Venus* results are important for comet work because the mechanisms of tail formation are thought to be very similar in comets and in Venus (Russell *et al.* 1982). Additional evidence is provided by recent MHD computer simulations of the comet–solar wind interaction by Fedder, Brecht, and Lyon (1981) and by Schmidt and Wegmann (1980); these studies support the essentially interplanetary values derived for the distant tail by Ershkovich (1976, 1978, 1979, 1980, 1982).

The present work addresses a possible visible manifestation of the magnetic field distribution in a cometary plasma tail: the tail should flare (i.e., increase in cross section with distance from the head) according to hypersonic

[1] On leave from the Department of Geophysics and Planetary Sciences, Tel-Aviv University.

pressure balance if the thermal plus magnetic pressures in the tail exceed those of the solar wind, and the extent of flaring should be the signature of the magnitude of the field gradient. It is our experience, unfortunately, that flaring angles are among the most difficult to measure, and are also among the least published, of comet-tail properties. However, from an analysis of Joint Observatory for Cometary Research (JOCR) photographs of recent bright comets, we have been able to make a number of flaring measurements (§ II), and they serve as the basis for the analysis given in § III. The most important observational result is that the flaring angle can vary to such an extent that on some days the flaring phenomenon is extremely visible, whereas on other days the tail is practically cylindrical in shape (i.e., there is no flaring). This difference in flaring is shown below to be governed by the plasma tail gas pressure and by the magnetic field strength at the flanks of the cometary ionopause.

II. FLARING OF COMETARY PLASMA TAILS

a) *Introduction*

So far as we know, no exhaustive investigation has yet been undertaken which examined the observed plasma tail morphology of *many* comets during *quiet* times. This lack of a single (or small number of) source(s) containing basic measurements (tail widths, flaring angles, etc.) is unfortunate since it is the comet–solar wind interaction in *steady state* which is properly the first target of theoretical work. (The study of *disturbed* plasma tails involves, more than any other class of activity in these tail systems, the phenomenon of *disconnection events* [DEs], and these have been studied in detail by Niedner and Brandt [1978, 1979, 1980] and cataloged by Niedner [1981].) The reader should bear this in mind and also recognize that the following developments and ideas are mostly meant to pertain to times when a comet is not undergoing rapid change.

Ershkovich (1976) pointed out that if a comet tail were generally similar to the geomagnetic tail, then one could expect the comet tail to flare out in a direction away from the head as a result of hypersonic pressure balance between the tail and the external solar wind. The amount of published observational material available to compare with such a hypothesis is not large, and Ershkovich was essentially limited to measurements of comet Arend-Roland 1957III on 1957 May 5. These data (made available via a private communication from F. D. Miller) revealed no flaring on the day in question, i.e., the tail width was independent of distance.

In contrast to this result were data contained in a later study of comet Tago-Sato-Kosaka 1969IX by Miller (1979). Wide-field photographs spanning a nearly 3 week interval in 1969 late December and 1970 January showed that on most days the form of the plasma tail was that of a wedge subtending, on the average, an angle $\epsilon \approx 4°$. In addition to these rather unique flaring data, Miller's paper contained measurements of several fundamental tail properties such as aberration angle, tail ray turning rates, etc.

In order to familiarize ourselves directly with the flaring phenomenon, as well as to extend the investigation of this property to a larger number of comets, we examined in detail a portion of the JOCR plate collection. The JOCR, located near Socorro, New Mexico (refer to Brandt *et al.* 1975 for details), has been in operation since late 1973 and has obtained wide-field ($8° \times 10°$) plates of four bright comets which have appeared since 1973: comets Kohoutek 1973f, Bradfield 1974b, Kobayashi-Berger-Milon 1975h, and West 1975n. We examined the plate material of the first two of these comets, with special emphasis on the flaring question, and the results are presented below.

b) *Comets Kohoutek 1973f and Bradfield 1974b*

Visual examination of the plates showed that on many nights the tail could be considered as flaring, although some of the flaring day assignments were uncertain due to the proximity to the tail of side rays, to disturbances in the main tail, etc. The adverse influence of rays and tail disturbances in the detection and measurement of flaring can be summarized as follows. Tail rays are known to be initially visible at rather large inclination angles ($\sim 50°$) with respect to the tail and then to turn toward it at a rate of a few degrees per hour (at large inclinations; the angular speed decreases, however, toward the tail axis); 15–25 hours after the first appearance of a ray, it merges with the main tail (Wurm and Mammano 1972). The complication due to side rays is that a symmetric, nearly closed ray pair may create the impression of a strongly flaring tail when in fact the actual tail is either flaring very much less or not at all. The problem posed by tail disturbances is obvious: the flaring angle is difficult to measure, and flaring itself is difficult to detect, when the tail borders are wavy and distorted. Moreover, because we are essentially only interested in the flaring which results from steady conditions both in the solar wind and in comet tails (refer to the earlier remarks in this section), "disturbance days" can be rejected on other grounds.

Four plates—two of each comet—were judged to be favorable in the context of the above considerations and were examined in detail; the resulting flaring measurements serve as the observational basis for the remainder of the paper. The procedure was as follows. Deep (i.e., high-density), high-contrast images were printed on Kodak Polycontrast matte paper from intermediate film copies, and tail width measurements were then made directly from the prints using pencil and ruler. Eight or twelve tail width measurements were made for each plate, the locations of the measurements along the tail depending solely on our confidence to make an accurate measurement (at some locations the tail borders were very diffuse, for example, and measurements of such tail segments were avoided as much as possible). It was felt that eight carefully selected points would be sufficient to reveal the general flaring trend of the associated tail images (see, for example, Table 1 of Ershkovich 1976, and Table 3 of Miller 1979). Our desire was to make measurements both as close to and as far from the head as possible; this we found to be impossible to accomplish with one print since the density range of the cometary images (from head to outer tail) far exceeded the dynamic range of the photographic paper. Hence, enlargement prints (2–3 per plate, printed to similar density and contrast) were made of various tail segments, which procedure optimized the measurements of each region of the tail. In this way we obtained tail widths very near the head center (well within the bright dust envelope of comet Kohoutek, for example) and to distances greater than 10^7 km from the head as well. (It is to be noted in this regard that the panel photographs in Fig. 1 [Plate 8] [discussed below] merely serve to show the large-scale morphology of the tail images—the measurements were not actually made from these specific images.)

Microdensitometry was considered as a possible alternative to the photographic print method described above but was rejected on several grounds. First, the JOCR plates of comets Kohoutek and Bradfield are uncalibrated and show, in some cases, a significantly nonuniform background which would render suspect the measurements of tail widths out to some chosen density level. Second, we considered that, although the application of densitometry might result in larger tail widths (Miller 1979 reports that densitometry of the tails of comets Arend-Roland 1957III and Tago-Sato-Kosaka IX resulted in tail widths approximately twice those obtained from visual inspection of plates), it would almost certainly not yield different tail *shapes* from those obtained using the print method.

Perhaps the best example of "quiet-time flaring" in comet Kohoutek occurred on 1974 January 14, and a JOCR photograph taken on that day is presented in Figure 1*a*. The scale appearing below the tail in this and the other photographs in the figure denotes a distance of 10^6 km derived on the assumption that the plasma tail was oriented along the prolonged radius vector. The tick marks above and orthogonal to the tail indicate positions at which the projected tail width was measured; the measurements are listed in Table 1. The growth of the tail width with distance is obvious both in Figure 1*a* and in Table 1; note that observations were made to within 6×10^5 km from the head center, and out to a distance of 1.5×10^7 km. It is further worth stating that the inner $\sim 2 \times 10^6$ km of plasma tail was embedded within the envelope of the dust tail, but that the superposition did not appear to degrade greatly the visibility of the plasma tail borders. Linear regression of the data applied to a radius-distance relationship of the form:

$$R = z \tan \epsilon/2 + R_0 \tag{1}$$

yielded $\epsilon = 1.^\circ9$ and $R_0 = 13{,}200$ km, with a correlation coefficient of $r^2 = 0.916$. Note that what is derived here is an *average* flaring angle over the entire measured length of the tail. While this tends to hide the effect of small-scale structures, it seems to us a justifiable procedure in view of the obviously *large-scale* flaring nature of the tail. As will become clear in § III, it is exactly the large-scale flaring of comet tails that our model addresses.

In contrast to the unambiguous flaring present on January 14 is the nearly total absence of it only 3 days later on January 17; a JOCR photograph of the comet on the latter date is presented in Figure 1*b*. Note from an inspection of both the figure and the tail width measurements in Table 1 that the tail inward of 7.1×10^6 km exhibited almost no detectable flaring: linear regression applied to this inner tail section (using eq. [1]) yields $\epsilon \leq 0.^\circ4$, $R_0 = 32{,}500$ km, and $r^2 = 0.080$. On our large-format prints of this region of the tail, much medium-scale and fine-scale structure can be seen—especially kinks and waves—and the tail width varies widely, showing no trends with distance. It should be pointed out, however, that, at a distance of $z \approx 7.5 \times 10^6$ km, the tail does widen suddenly to a width of $\sim 3.4 \times 10^5$ km, and it steadily thickens out to the last measured point at $z \approx 1.7 \times 10^7$ km.

TABLE 1

DIAMETERS, $2R$, OF THE PLASMA TAILS OF COMETS KOHOUTEK 1973f AND BRADFIELD 1974b VERSUS DISTANCE Z FROM THE NUCLEUS

Comet Kohoutek, 1974 Jan 14		Comet Kohoutek, 1974 Jan 17		Comet Bradfield, 1974 Mar 23		Comet Bradfield, 1974 Apr 9	
z (km)	$2R$ (km)	z (km)	$2R$ (km)	z (km)	$2R$ (km)	z (km)	$2R$ (km)
5.8×10^5	5.3×10^4	1.28×10^6	5.3×10^4	6.8×10^5	2.6×10^4	6.7×10^5	5.1×10^4
2.25×10^6	8.2×10^4	2.01×10^6	5.3×10^4	1.13×10^6	4.9×10^4	1.66×10^6	8.9×10^4
4.25×10^6	2.2×10^5	2.57×10^6	1.3×10^5	2.10×10^6	1.2×10^5	2.98×10^6	9.3×10^4
6.34×10^6	2.6×10^5	3.56×10^6	7.0×10^4	3.20×10^6	1.5×10^5	4.34×10^6	1.6×10^5
8.13×10^6	2.3×10^5	4.74×10^6	7.0×10^4	4.92×10^6	3.4×10^5	5.29×10^6	1.1×10^5
9.89×10^6	3.0×10^5	5.33×10^6	1.9×10^5	7.99×10^6	4.8×10^5	7.00×10^6	1.3×10^5
1.22×10^7	3.8×10^5	6.31×10^6	1.1×10^5	9.73×10^6	5.1×10^5	8.84×10^6	1.7×10^5
1.51×10^7	5.9×10^5	7.08×10^6	6.2×10^5	1.09×10^7	5.9×10^5	1.18×10^7	3.4×10^5
		8.27×10^6	3.4×10^5				
		1.08×10^7	5.2×10^5				
		1.39×10^7	5.6×10^5				
		1.70×10^7	6.5×10^5				

Our interpretation of this double character of the tail is that the outer portion may contain *detached* plasma and magnetic flux, which gives it a thicker appearance, whereas the inner section contains plasma running down magnetic flux which is uniformly attached to the head region. For future analysis we will consider this tail to be non-flaring, with the understanding that the innermost eight measurements (out to $z = 7.1 \times 10^6$ km) are being referred to.

The most dramatic flaring difference we observed occurred in comet Bradfield 1974b on 1974 March 23 and April 9. On the former date (a JOCR photograph taken then is presented in Fig. 1*c*), flaring is unmistakable and is seen to persist for much of the entire visible length of the plasma tail (some 1.6×10^7 km). The last point at which a tail width measurement could confidently be made was at $z \approx 1.09 \times 10^7$ km; beyond this the tail is too faint and diffuse to measure. Least squares application of equation (1) suggests $\epsilon = 3^\circ.2$ and $R_0 = -385$ km, with $r^2 = 0.976$. Note the very high correlation coefficient, which indicates that a (nearly) constant flaring angle existed over the distance range of the measurements. The negative value for R_0 is, of course, nonphysical; further discussion of the meaning of R_0 will be given in § III*b*.

In marked contrast was the situation some 2.5 weeks later, on April 9. Figure 1*d* and Table 1 show that the tail was narrow and essentially cylindrical in shape. A regression analysis of all measured points yields $\epsilon = 1^\circ.2$ and $R_0 = 14{,}750$ km, with $r^2 = 0.782$. Almost all of this modest degree of flaring results from the innermost and outermost measurements, however. Equation (1) applied to the middle 6 data points (which span 64% of the total z-range measured) yields $\epsilon = 0^\circ.005$ and $R_0 = 38{,}450$ km, with $r^2 = 0.572$. For the purposes of the following analysis, we will consider this tail to be (essentially) nonflaring.

Out of concern that perhaps transient events in the solar wind—such as high-speed streams and compression regions—might have been responsible for some of the differences in flaring, hence violating our original intention to study only quiet-time plasma tails and solar wind, we examined the state of the solar wind at the times of the photographs in Figure 1 by utilizing the spacecraft data atlas assembled by J. King (1977). Early 1974 was a time of exceptionally complete in situ monitoring of the solar wind (refer to King's atlas); by corotating the data to the respective comets using the corotation procedure described by Niedner, Rothe, and Brandt (1978), we were able to satisfy ourselves that on all four dates, comets Kohoutek and Bradfield were in all likelihood immersed in the reasonably steady solar wind which is found between successive high-speed streams. We felt that this procedure (i.e., corotating near-Earth solar wind observations to the comets) was a reasonable one since the cometary heliographic latitudes were not large. Table 2 lists the heliocentric distance and heliographic latitude of the comets at the times in question, the time at Earth which corotates to the times of the comet photographs, and a description of the solar wind at the appropriate Earth time frame.

We would summarize our findings about the flaring of comets 1973f and 1974b as follows. On most days, *some* degree of flaring was present (this was the case for both comets), although the flaring angle was sometimes rather difficult to measure due to the presence of disturbances or folding tail rays. When such a measurement could be made with confidence, the value was typically in the vicinity of a few (2°–4°) degrees, in agreement with Miller's (1979) results. There were a few days on which the flaring was essentially zero (e.g., Figs. 1*b* and 1*d*), and thus the flaring of cometary plasma tails is subject to a wide range of observed behavior. An additional property which proves to be of some interest in the next section is the scale length along the tail over which flaring can occur: the photographs presented in Figures 1*a* and 1*c* (and particularly 1*c*) strongly suggest that flaring persisted for several times 10^6 km (also refer to Table 1).

III. A MODEL FOR COMETARY FLARING

a) *Introductory Remarks*

For steady state situations, we consider the cometary magnetic field to be related to conditions in the solar wind via the equation of hypersonic pressure balance applied along the cometary ionopause:

$$(K\rho V^2 \sin^2 \alpha + p + B^2/8\pi)_\infty = (p + B^2/8\pi)_i \,, \tag{2}$$

where ρ, V, and p are, respectively, the plasma density, bulk velocity, and gas kinetic pressure, α is the angle between the solar wind velocity and the ionopause, and the indices ∞ and i refer, respectively, to the undisturbed solar wind

TABLE 2

GEOMETRICAL AND SOLAR WIND CIRCUMSTANCES FOR COMETS KOHOUTEK 1973f AND BRADFIELD 1974b AT THE TIMES OF FIGURES 1*a*–1*d*

Comet	Date (yr/mo/d)	r (AU)	b	t_E	Remarks about Solar Wind
1973f................	74/1/14	0.605	$+6^\circ.9$	1/19	moderate speed (500 km s^{-1}), low density (5 cm^{-3})
1973f................	74/1/17	0.685	$+5^\circ.6$	1/22	
1974b...............	74/3/23	0.516	$-14^\circ.0$	3/28	
1974b...............	74/4/9	0.715	$+26^\circ.3$	4/12–13	

and the cometary ionopause. The coefficient K decreases from 0.844 for Mach numbers $M \gg 1$ to 0.625 with $M = 1$ if the ratio of specific heats equals 2 (see Spreiter and Alksne 1969). Equation (2) has been used successfully by Sonett, Mihalov, and Klozenberg (1971) to model the large-scale shape of the geomagnetic tail and has been shown to hold along the Venusian ionopause (Vaisberg, Intriligator, and Smirnov 1981).

The maximum value of the magnetic field in the cometary environment occurs at the stagnation point ($\alpha = 90°$), and insertion into equation (2) of typical quiet-time solar wind parameters at 1 AU yields $B_{st} \approx 50\gamma$. By taking the projection of the MHD momentum equation across the fan-shaped magnetic field lines (identified with the tail rays), it is possible to show that the surfaces of constant total pressure, $p + B^2/8\pi = \text{const.}$, are approximately coincident with those normal to B, and therefore that they intersect the ionopause; hence, the magnetic field in the cometary ionosphere does not exceed B_{st} (Ershkovich 1979, 1982).

At the distant ionopause the total pressure, decreasing away from the stagnation point, should approach that of the undisturbed solar wind: $(p + B^2/8\pi)_i \to (p + B^2/8\pi)_\infty$, and pressure balance across the distant tail yields:

$$(p + B^2/8\pi)_T = \text{const.} \approx (p + B^2/8\pi)_\infty \, . \tag{3}$$

Since $p_\infty \approx B_\infty^2/8\pi$, one obtains the field in the distant tail: $B_T \lesssim 2^{1/2} B_\infty \approx 10\gamma$ at 1 AU, in agreement with the value derived from observations of helical waves. Numerical simulations of the solar wind interaction with comets performed by Fedder, Brecht, and Lyon (1981) confirm these estimates. Numerical calculations by Schmidt and Wegmann (1980, 1982) yield approximately the same field values in the comet tail, but the magnetic field at the stagnation point, B_{st}, turned out to be about 130γ (at 1 AU, under typical conditions). This increase (by a factor of 2.6 over the value of B_{st} estimated from eq. [2]) is caused by the high curvature of the magnetic field lines along the stagnation streamline and, as such, this local effect should vanish away from the stagnation point, the estimate of the comet tail field being unchanged.

(The huge pileup of the magnetic field lines at the stagnation point obtained by Schmidt and Wegmann 1982 seems to be associated with their assumption that the ionopause is a rigid surface with a small radius of curvature at the stagnation point. In reality, the cometary ionopause should undergo the interchange instability. As a result, the interplanetary magnetic field lines penetrate the ionopause, and the nonzero magnetic field appears on the right-hand side of eq. [2]. According to the general Le Chatelier principle, the radius of curvature of magnetic field lines should increase due to the instability, diminishing the pileup effect. In contrast to Schmidt and Wegmann 1980, 1982, the numerical calculations by Fedder, Brecht, and Lyon 1981 are compatible with an ionopause as a free surface. As a result, they obtained $B_{st} \approx 48\gamma$, in agreement with the value derived from eq. [2].)

The decrease of the cometary field strength from values near 50γ in the head to $\leq 10\gamma$ in the distant tail should be accompanied by flaring of the tail if the magnetic flux in each tail lobe is approximately conserved, i.e., if $BR^2 \approx \text{const.}$, where R is the tail radius. Strictly speaking, the ionopause conserves magnetic flux only if it is a tangential discontinuity surface. It is clear from the properties of folding tail rays, however, that neither condition holds completely: in the region where the ray closure occurs, magnetic field lines (identified with the rays) penetrate the ionopause, the tail rays being observed at several times 10^6 km from the tail axis. Thus the ionopause should be treated as a contact rather than a tangential discontinuity surface in this region, magnetic flux conservation in the main tail being violated.

Miller (1979), however, pointed to the fact that the folding rays seem to lie very nearly in the same plane: if they were distributed at random about the axis, one might expect to find short "young" rays projected closer to the axis than the longer "older" rays are, which is not the case. Hence the solid angle through which the field lines "escape" through the ionopause should be small, and flux conservation approximately holds. Thus the majority of the ionopause could be considered approximately as a tangential discontinuity surface.

b) Numerical Calculations

The gradient of the tail width expected on the basis of hypersonic pressure balance is easily obtained from equation (2):

$$\frac{dR}{dz} = \tan \alpha = \left[\frac{8\pi(p_i - p_\infty) + (B_i^2 - B_\infty^2)}{8\pi K \rho_\infty V_\infty^2 - 8\pi(p_i - p_\infty) - (B_i^2 - B_\infty^2)}\right]^{1/2} . \tag{4}$$

Note that the angle α, defined in § III*a*, is half the flaring angle (i.e., $\alpha = \epsilon/2$). Inspection of equation (4) shows that tail flaring is expected at any point for which the tail pressure is large enough to satisfy $B_i^2 + 8\pi p_i > B_\infty^2 + 8\pi p_\infty$. Failure to satisfy this inequality means that the external magnetic and gas kinetic pressures are sufficient to balance the comet-tail pressure *without* any contribution from the dynamic pressure of the solar wind; in this situation there would be no flaring and the tail would be cylindrical in shape at the location in question.

Equation (4) may be rewritten in the following way to incorporate conservation of tail magnetic flux:

$$\frac{dR}{dz} = \left[\frac{8\pi[n_{i,0} kT_{i,0} - p_\infty] + [B_{i,0}^2(R_0/R)^4 - B_\infty^2]}{8\pi K \rho_\infty V_\infty^2 - 8\pi[n_{i,0} kT_{i,0} - p_\infty] - [B_{i,0}^2(R_0/R)^4 - B_\infty^2]}\right]^{1/2} , \tag{5}$$

Here, $n_{i,0}$ and $B_{i,0}$ are the plasma density and tail field strength at some reference distance where the tail width is R_0, and $T_{i,0}$ is the temperature sum of tail ions and electrons at the same location. The solar wind speed, as well as its gas and magnetic pressures, have all been assumed to be constant down the tail.

Note that equation (5) takes $n_i T_i = \text{const.}$; in other words, the gas pressure in the tail is assumed to be independent of distance from the head. The justifications for this approach are as follows. First, it is clear that n_i and T_i have qualitatively *opposite* trends with distance: n_i should decrease outward due both to an increase in tail radius (when the tail flares) and to ion acceleration down the tail (since $n_i V_i R^2 = \text{const.}$), whereas T_i must *increase* as a result of heat transfer from a hot plasma (solar wind, $T_\infty > 10^5$ K) to a cold one (tail ions, $T_{i,0} \approx 10^4$ K). Although a detailed treatment of these two competing effects is beyond the scope of this paper, it is worth mentioning that an empirical argument can be made for taking $n_i T_i \approx \text{const.}$: for nonflaring tail systems (e.g., comet Bradfield on 1974 April 9), $\alpha = \text{const.} = 0°$ *requires* $n_i T_i \approx \text{const.}$ since, on the assumption of magnetic flux conservation, the tail magnetic field does not change when $R = \text{const.}$; pressure balance (eq. [2]) thus requires $p_i = \text{const.}$ The situation for flaring tails is necessarily less clear, and we have simply assumed $n_i T_i \approx \text{const.}$ for this case as well (a short discussion is given at the end of this section to models generated under the assumption that $T_i = \text{const.}$). Thus, our approach is to assume that any changes in the flaring angle with distance down the tail are controlled (almost) *entirely* by the decrease of the tail magnetic field strength with distance from the head. This assumption has also been made in treatments of the shape of the geomagnetic tail (e.g., Sonett, Mihalov, and Klozenberg 1971).

Equation (5) was used to calculate theoretical flaring angles and the relationship between R and z by assuming that the solar wind conditions were $n_\infty = 10\ \text{cm}^{-3}$, $V_\infty = 400\ \text{km s}^{-1}$, $B_\infty = 7\gamma$, and $T_\infty = 3 \times 10^5$ K; these values were thought to be appropriate for the quiet-time solar wind at 0.6–0.7 AU. We chose as our "reference point" the distance $z = 0$, i.e., the flanks of the sunlit ionopause; the tail radius at that point, R_0, is a free parameter to be determined by fitting observations to the model. We chose for the tail temperatures the value $T_{i,0} = 10^4$ K.

Figures 2 and 3 show the α versus log z (*upper*) and log R versus log z (*lower*) relationships for a variety of field strengths at the flanks of the ionopause (Fig. 2) and a range of ionopause densities (Fig. 3). To show general trends among the theoretical curves, R_0 was for the sake of illustration chosen to be 20,000 km (the observations will be presented later). It should be noted that $z = \int dR/(dR/dz)$, where dR/dz is given by equation (5), is a hyperelliptic integral and hence could not be integrated analytically; a computer program was written to calculate the integral numerically. The end points of the curves in Figures 2 and 3 denote those distances at which the tail stops flaring ($\alpha = 0°$, $R = \text{const.}$) as a result of the radial decrease of B_i (the two curves which extend outside the right ordinate in Fig. 3 have a different explanation; see below).

Figure 2 shows that, for fixed $n_{i,0}$ ($= 300\ \text{cm}^{-3}$), the value of $B_{i,0}$ can control the magnitude of the flaring angle, the distance down the tail to which flaring extends, and the final width achieved by the tail. For example, increasing $B_{i,0}$ from 10γ to 50γ results in a $\sim$2.25 increase in tail width and a 3.5 enhancement in the flaring length of the tail (a mechanism by which $B_{i,0}$ can vary in an individual comet is presented in § IV). These are relatively minor effects, however, compared with the changes encountered when keeping $B_{i,0}$ fixed and varying $n_{i,0}$. Figure 3 shows that

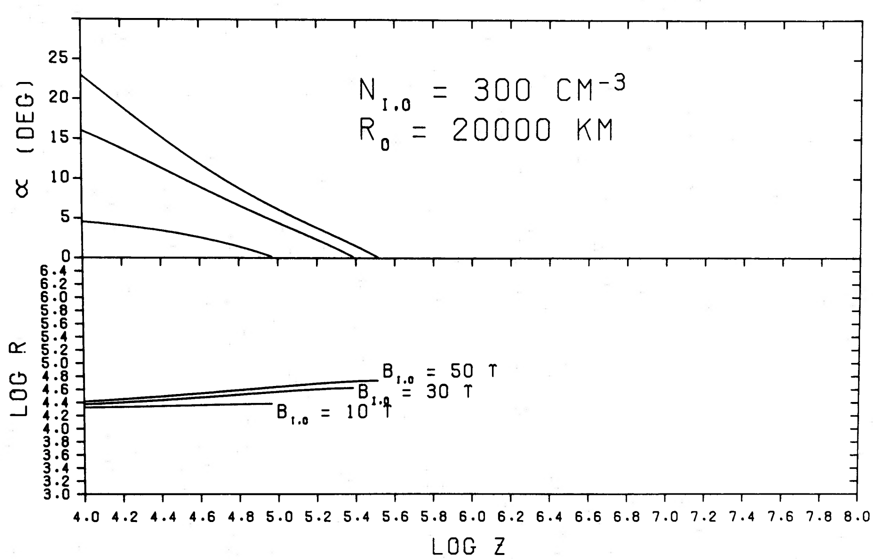

FIG. 2.—Model-generated flaring angles (*upper*) and the log R–log z (radius-distance) relationship (*lower*) for the case in which the tail ion density at the flanks of the ionopause, $n_{i,0}$, is 300 cm^{-3}. The curves in each panel were obtained by varying the magnetic field strength at the flanks of the ionopause, $B_{i,0}$, between 10γ and 50γ (see lower panel; although unlabeled, the flaring angle curves in the upper panel are for the same $B_{i,0}$ and descend in sequence from 50γ to 10γ).

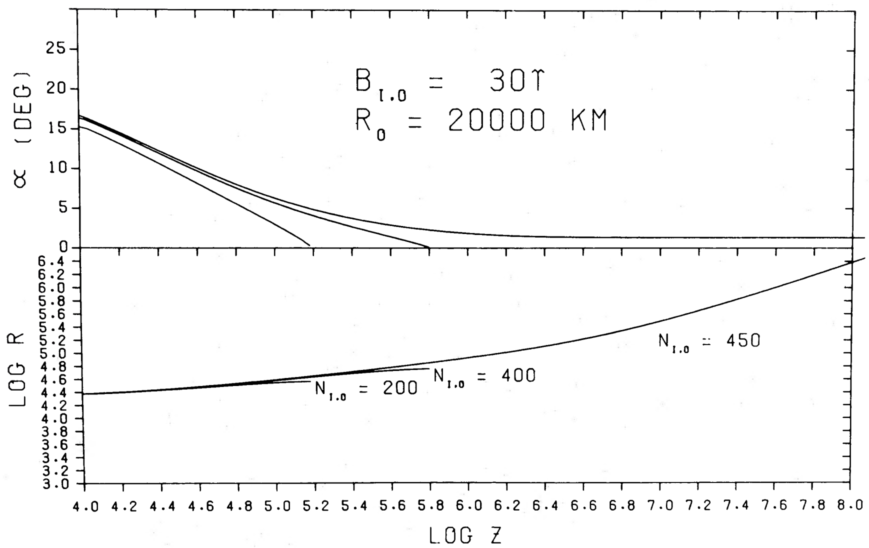

FIG. 3.—Same as Fig. 2, except that the ion density at the flanks of the ionopause, $n_{i,0}$, is varied, while $B_{i,0}$ is held fixed at 30γ. Note that flaring continues out past log $z = 8.0$ when $n_{i,0} = 450$ cm^{-3}, whereas flaring is contained within log $z < 6.0$ for the smaller densities.

a substantial growth in the flaring lengths is encountered by increasing $n_{i,0}$ from 200 to 400 cm^{-3}. In the former case, flaring extends only to $\sim 1.5 \times 10^5$ km down the tail and would almost certainly *not* be visible in wide-field photographs (e.g., Figs. 1*b* and 1*d*). On the other hand, for $n_{i,0} = 400$ cm^{-3}, flaring extends to $\sim 6.5 \times 10^5$ km and might be visible (note, however, that prominently flaring tails—e.g., Figures 1*a* and 1*c*—have flaring lengths of *at least* 6–8 $\times 10^6$ km).

Our model predicts the existence of a *threshold* in $n_{i,0}$, above which the tail essentially never stops flaring; Figure 3 shows one such case, $n_{i,0} = 450$ cm^{-3} (the continuation of the curves through the right ordinate is meant to convey the persistence of the flaring phenomenon). The cause of this threshold effect is not difficult to isolate: the assumption of constant gas pressure in the tail results in a critical value for $n_{i,0}$ such that:

$$(n_{i,0})_c kT_{i,0} = p_\infty + B_\infty^2/8\pi \, . \tag{6}$$

In effect, what this condition means is that the plasma tail gas pressure can balance the solar wind pressure even when $B_i = 0$; for densities exceeding the critical value, the tail flares "forever" with a terminal flaring angle given by:

$$\alpha_t = \sin^{-1}\left[\frac{n_{i,0} kT_{i,0} - p_\infty - B_\infty^2/8\pi}{K\rho_\infty V_\infty^2}\right]^{1/2} . \tag{7}$$

Insertion into equation (7) of $n_{i,0} = 450$ cm^{-3} and the values listed earlier for the tail and the solar wind results in $\alpha_t = 1\overset{\circ}{.}3$; the asymptotic approach to this value (which is comparable to that observed in comets Kohoutek and Bradfield on flaring days) is shown in Figure 3. At this point it is worth mentioning that models were run in which T_i = const., the tail gas pressure thus varying as $1/R^2V_i$, where V_i is the ion flow speed down the tail. It was found in all cases (i.e., for all reasonable input combinations of $B_{i,0}$ and $n_{i,0}$) that flaring stopped inside of 1–2 $\times 10^5$ km from the head, in disagreement with observations of plasma tails on flaring days.

A detailed comparison of the observations in Figure 1 (summarized in Table 1) with the flaring model adopted here is not unambiguous: there is some uncertainty in R_0 and, moreover, because the small flaring portion of an observed nonflaring tail (i.e., the innermost 1–2 $\times 10^5$ km) is itself unobserved, the final tail width measured from a photograph can be satisfactorily reproduced by several different ($B_{i,0}$, $n_{i,0}$) combinations for a given choice of R_0. Even for flaring tails, measurements of ϵ (or α) only yield $n_{i,0}$ (assuming $T_{i,0}$, p_∞, etc., are correct); the tail shape still can be accurately modeled by different (R_0, $B_{i,0}$) pairs (note in this regard that R_0 essentially sets the scale of the tail system).

Despite these limitations, we have attempted to model the observations (Fig. 1, Table 1) as well as possible, and the results are shown in Figures 4–7. The asterisks in the lower panel of each figure represent the observed tail widths and distances listed in Table 1, and one figure is devoted to each of the photographs in Figure 1. Three families of curves, $B_{i,0} = 10\gamma$, 30γ, and 50γ, are plotted in each figure. The values of $n_{i,0}$ in Figures 4 and 6 (comet Kohoutek on January 14, and comet Bradfield on March 23: both flaring days) were those which resulted from combining the least squares solutions of tan $\epsilon/2$ in equation (1) with the $\alpha_t(n_{i,0})$ relationship in equation (7) (recall that $\alpha = \epsilon/2$). Since the photographs represented by Figures 5 and 7 were of *nonflaring* tail systems, a nominal value of $n_{i,0} = 300$

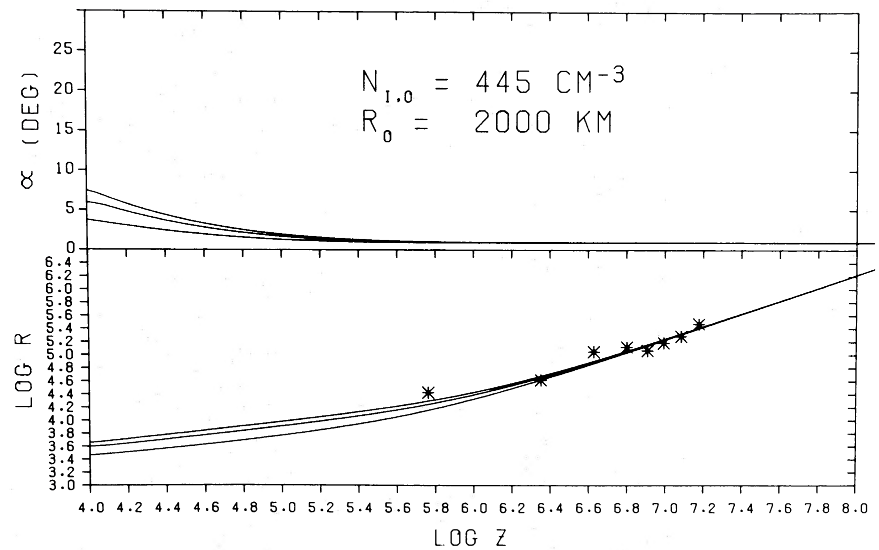

FIG. 4.—Flaring model curves and observations (*asterisks*) of comet Kohoutek 1973f on 1974 January 14 (Fig. 1*a*, Table 1). The three model curves in each panel are for (*top to bottom*) $B_{i,0} = 50\gamma$, 30γ, and 10γ, and all model curves use $n_{i,0} = 445$ cm^{-3} and $R_0 = 2000$ km. Note the good agreement between the model and the observations of this flaring tail.

cm^{-3}—below the large-scale flaring threshold—was used. The vertical tick marks along the log R—log z curves in Figures 5 and 7 indicate those positions where flaring stops; the curves have been continued at constant R out to large z for comparison with the observations.

For all four figures, the quoted R_0 was that which brought about a close agreement between the observations and the model. The reader will quickly note that these are *not* the same R_0 values as those obtained in the least squares analysis which utilized equation (1) (refer to § II*b*). The reason is simply that equation (1) assumed a *constant* flaring angle, even at small z. Figures 2–7 show that constant flaring is decidedly *not* the case for small z in the model calculations; hence, the discrepancies between the two sets of R_0 are not surprising.

The agreement between the model calculations and the observations is good, but it should be stated that the model curves are not best fits in the least squares sense. The reason is that, without any analytical expression for $R(z)$, a regression analysis could have proceeded only with the generation of a grid of many (computer-time consuming)

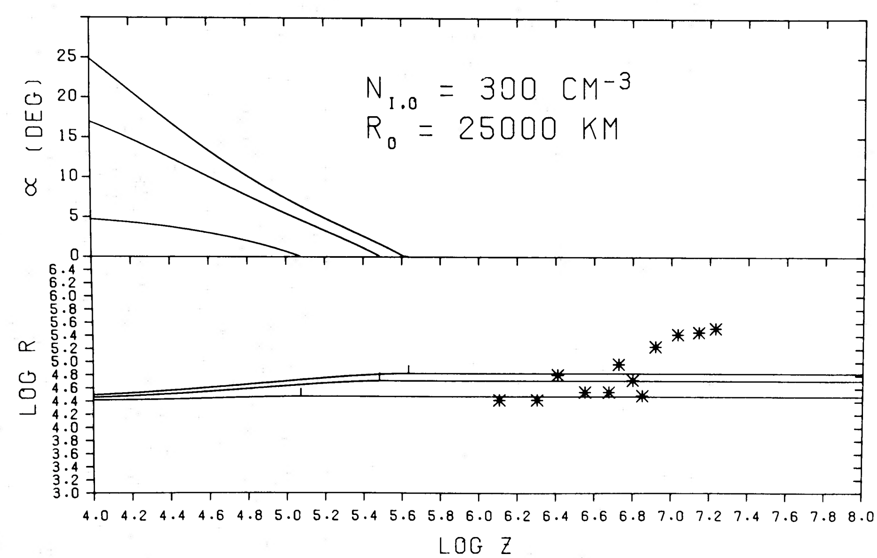

FIG. 5.—Essentially the same format as Fig. 4, except that the vertical tick marks on the log R–log z curves denote those distances at which model flaring stops; the curves were continued at constant R out to large z for comparison with observations of comet Kohoutek on 1974 January 17 (Fig. 1*b*). Note that the four outermost observations are not well represented and were in fact not used in the derivation of this $n_{i,0} = 300$ cm^{-3}, $R_0 = 25{,}000$ km model (refer to § II*b* for a discussion).

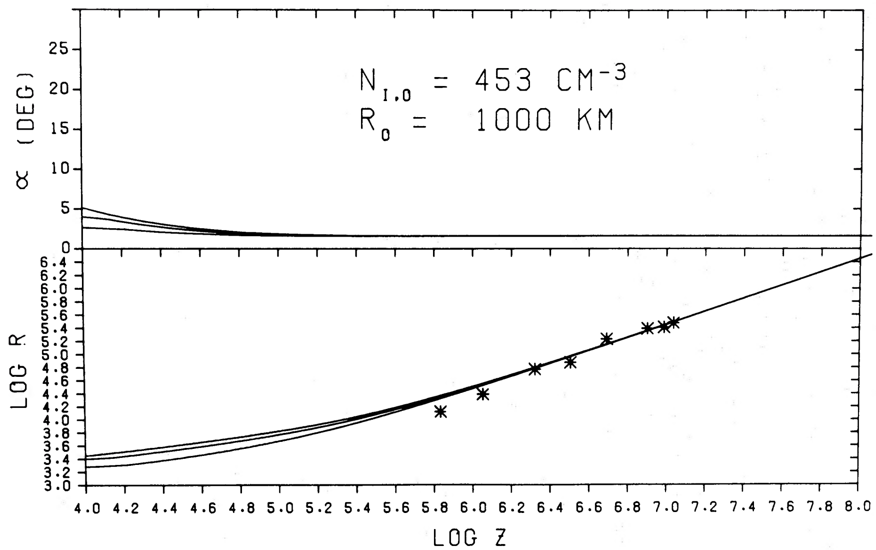

FIG. 6.—Same format as Fig. 4; the observations are of the flaring tail of comet Bradfield 1974b on 1974 March 23

models. We found that a visual inspection of figures generated using two or three widely disparate sets of inputs (per photograph) allowed us to determine a "best fit" without much trouble, and Figures 4–7 are the result of such a procedure.

Although they are plotted in Figure 5, the four outermost measurements of the tail of comet Kohoutek on January 17 are not deemed physically important to the present analysis (refer to § II*b* for a discussion), and hence they have not been considered in the model-fitting procedure. Note that the seeming contradiction of having *larger* flaring angles at small *z* on *nonflaring* days (Figs. 5 and 7 vs. Figs. 4 and 6) is really not a contradiction at all. Recall that R_0 is a kind of "scaling factor" and that, all other things (i.e., inputs to the model) being equal, the flaring angles depend only on the value of (R_0/R). Our analysis suggests that, on nonflaring days, R_0 was an order of magnitude *larger* than on flaring days (compare, for example, Figs. 6 and 7), and this is the reason for the seemingly inverse behavior of the flaring angles.

The relatively small values of R_0 on flaring days ($R_0 \approx$ 1000–2000 km) is one of the most interesting (and perhaps surprising) results of this investigation, and the problem bears further study. Either compression of the ionosphere (i.e., a decrease of the nuclear distance to the contact surface) took place and favored flaring, or we have overestimated R_0 for nonflaring days by assuming that there was no large-scale flaring beyond a few $\times 10^5$ km (in other words, the introduction of a small, nonzero ϵ would tend to reduce R_0). Either situation would seem to be possible, in particular the former one, because a reduction in the size of the ionosphere necessarily implies higher ion densities

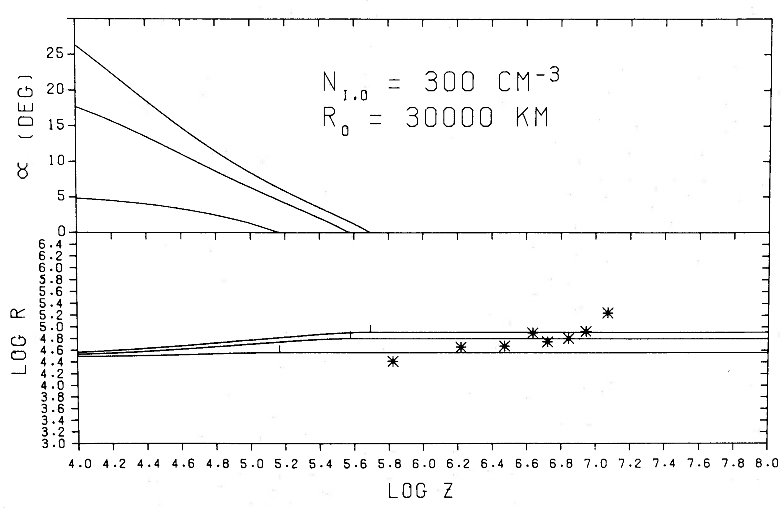

FIG. 7.—Same format as Fig. 5; the observations are of the nonflaring tail of comet Bradfield on 1974 April 9

along the ionopause (hence, a greater likelihood of large-scale flaring) if the ion production is constant. It is important to note, however, that Combi and Delsemme's (1980) spectroscopic work on comet West 1976VI (a considerably brighter object than either comet Kohoutek or comet Bradfield) suggested contact surface radii in the range from 1 to 3×10^4 km, much larger than the 1000–2000 km size derived for flaring days for the two comets under study. On the other hand, calculations by Houpis and Mendis (1980) indicate that for medium-bright comets like P/Halley, the contact surface may be at a distance of only $\sim$4000 km (not unlike the values obtained here for flaring days).

Despite the inherent uncertainties discussed above, what the model calculations suggest most strongly is that the flaring state of a cometary plasma tail is dependent (principally) on the ion tail gas pressure (i.e., $n_{i,0}$), and (secondarily) on the magnetic field strength at the flanks of the ionopause. Clearly, these are conditions in a comet which could be subject to large variations, thus explaining the significant observed differences in comet-tail flaring.

IV. DISCUSSION AND CONCLUSION

The results of the previous section showed that, if the gas pressure of the tail plasma is approximately constant with distance down the tail, then for densities large enough, the tail flares at least on scales greater than 10^7 km, and the hypersonic pressure balance flaring model is in satisfactory agreement with the observations presented in § II. It was further suggested that "flaring days" *may* be associated with an order-of-magnitude deflation of the cometary ionosphere, although the implications of this result are unclear and must await further analysis.

No measurements exist for $B_{i,0}$, the magnetic field strength at the flanks of the ionopause, and all we are reasonably confident of is that $B_{i,0} < B_{st}$ (recall that for quiet times in the solar wind near 1 AU, the stagnation field is $B_{st} \approx 50\gamma$). A recent paper by Houpis and Mendis (1981), however, contains results which show how $B_{i,0}$ might vary even for one constant value of the solar wind dynamic pressure ($B_{st} =$ const.). Briefly, these authors showed how the shape of the sunlit ionopause (or tangential discontinuity) depends critically on the ratio of the neutral and ion "stand-off" distances from the nucleus (r_0 and r_{i0}, respectively), and the distance R_c at which the ions and neutrals decouple collisionally. Houpis and Mendis found that, for a typical comet (with a nuclear radius of about 2.5 km) at the heliocentric distances 0.6 AU $< d <$ 3 AU and with a typical ionization time scale $\tau \approx 5 \times 10^5$ s, the inequality $r_0 > R_c > r_{i0}$ usually holds. In this case the tangential discontinuity will follow the R_c surface, which is spherical, rather than the "finger-shaped" r_{i0} curve (see Fig. 4 of Houpis and Mendis 1981, Case II). The reader should refer to Houpis and Mendis's paper for details, but briefly, the neutrals can communicate their momentum to the ions up to the distance R_c, and with $r_0 > R_c$ they have sufficient momentum to stop the solar wind at the distance R_c. If the sunlit ionopause is spherical, then at the flanks of the ionopause the angle between the solar wind velocity and the ionopause, α, is zero, and the hypersonic pressure balance equation is reduced to $(p + B^2/8\pi)_i = (p + B^2/8\pi)_\infty$, which has the same form as equation (3). Thus the magnetic field at the flanks of the cometary head is of the same order of magnitude as the magnetic field B_T in the distant tail. In this case, the cometary magnetic field, decreasing away from the stagnation point, already reaches the value B_T within the cometary head, and no further decrease along the tail axis is expected. Hence, there would be no systematic flaring effect.

On the contrary, if the ionization time scale drops to about 5×10^4 s because of some additional ionization processes, then $r_{i0} > R_c$, and the sunlit cometary ionopause will be "finger-shaped" or parabolic (Houpis and Mendis 1981, Figs. 3 and 4, Case Ia). In this case the magnetic field in the head still remains substantially greater than the B_T value in the distant tail. The decrease of the cometary magnetic field down to the B_T value in the distant tail will then be accompanied by tail flaring, the extent of which depends, as pointed out earlier, on $n_{i,0}$.

In summary, a model of cometary plasma tail flaring was presented which explains the observed variability in flaring on the basis of the gas pressure of tail ions and the strength of the magnetic field at the flanks of the cometary ionopause. Both properties depend on the location and shape of the cometary ionopause. The flaring angles generated by the hypersonic pressure balance model adopted here are in good agreement with observations of tail flaring in comets Kohoutek and Bradfield.

The research by A. I. Ershkovich has been performed under a Research Associateship of the National Research Council—National Academy of Sciences. We are grateful to the referee for constructive comments, which have greatly improved the quality of our paper.

REFERENCES

Alfvén, H. 1957, *Tellus*, **9**, 92.
Brandt, J. C. 1968, *Ann. Rev. Astr. Ap.*, **6**, 267.
Brandt, J. C., Colgate, S. A., Hobbs, R. W., Hume, W., Maran, S. P., Moore, E. P., and Roosen, R. G. 1975, *Mercury*, **4**, 12.
Brandt, J. C., and Mendis, D. A. 1979, in *Solar System Plasma Physics*, Vol. **2**, ed. C. F. Kennel *et al.* (Amsterdam: North-Holland), p. 258.
Combi, M. R., and Delsemme, A. H. 1980, *Ap. J.*, **238**, 381.
Ershkovich, A. I. 1976, *M.N.R.A.S.*, **177**, 649.
———. 1978, *M.N.R.A.S.*, **184**, 755.
Ershkovich, A. I. 1979, *Planet. Space Sci.*, **27**, 1239.
———. 1980, *Space Sci. Rev.*, **25**, 3.
———. 1982, *M.N.R.A.S.*, **198**, 297.
Fedder, J. A., Brecht, S. A., and Lyon, J. G. 1981, *Trans. Am. Geophys. Union, EOS*, **62**, 367.
Houpis, H. L. F., and Mendis, D. A. 1980, *Ap. J.*, **239**, 1107.
———. 1981, *Ap. J.*, **243**, 1088.
Hyder, C. L., Brandt, J. C., and Roosen, R. G. 1974, *Icarus*, **23**, 601.
Ip, W.-H., and Mendis, D. A. 1975, *Icarus*, **26**, 457.

Ip, W.-H., and Mendis, D. A. 1976, *Icarus*, **29**, 147.
King, J. 1977, *Interplanetary Medium Data Book* (Washington, D. C.: NASA National Space Science Data Center).
Mendis, D. A., and Morrison, P. J. 1979, *M.N.R.A.S.*, **188**, 727.
Miller, F. D. 1979, *Icarus*, **37**, 443.
Niedner, M. B., Jr. 1981, *Ap. J. Suppl.*, **46**, 141.
Niedner, M. B., Jr., and Brandt, J. C. 1978, *Ap. J.*, **223**, 655.
———. 1979, *Ap. J.*, **234**, 723.
———. 1980, *Icarus*, **42**, 257.
Niedner, M. B., Jr., Rothe, E. D., and Brandt, J. C. 1978, *Ap. J.*, **221**, 1014.
Russell, C. T., Luhmann, J. G., Elphic, R. C., and Neugebauer, M. 1982, in *IAU Colloquium 61, Comets: Gases, Ices, Grains, and Plasma* (Tucson: University of Arizona Press), p. 561.
Schmidt, H. U., and Wegmann, R. 1980, *Computer Phys. Comm.*, **19**, 309.
———. 1982, in *IAU Colloquium 61, Comets: Gases, Ices, Grains, and Plasma* (Tucson: University of Arizona Press), p. 538.
Sonett, C. P., Mihalov, J. D., and Klozenberg, J. P. 1971, *Cosmic Electrodynamics*, **2**, 22.
Spreiter, J. R., and Alksne, A. Y. 1969, *Planet. Space Sci.*, **17**, 233.
Vaisberg, O. L., Intriligator, D. S., and Smirnov, V. N. 1981, *Kosmich. Issled.*, **19**, 104.
Wurm, K., and Mammano, A. 1972, *Ap. Space Sci.*, **18**, 273.

John C. Brandt, Alexander I. Ershkovich, and Malcolm B. Niedner, Jr.: Laboratory for Astronomy and Solar Physics, NASA Goddard Space Flight Center, Greenbelt, MD 20771

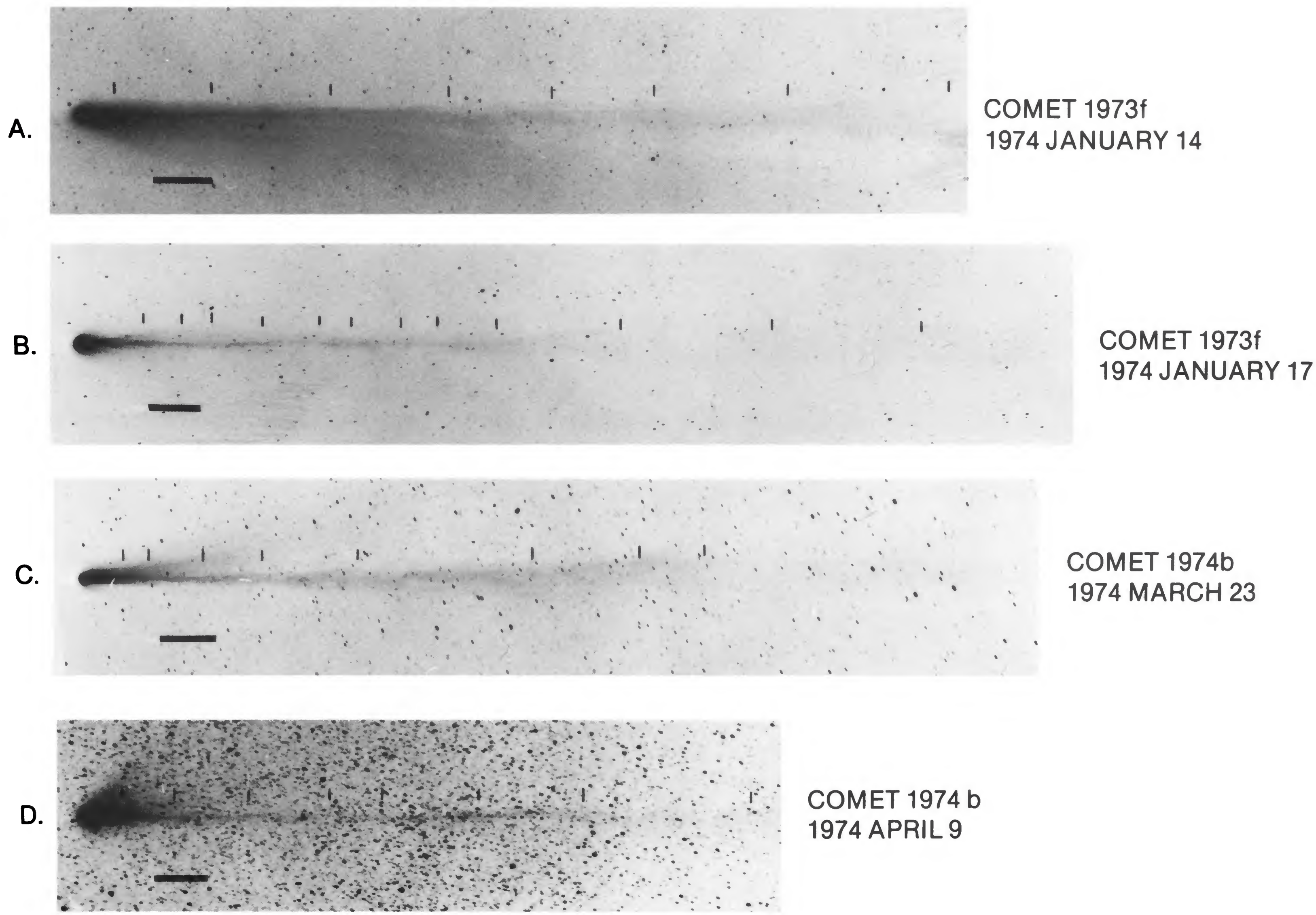

FIG. 1.—(*a*) JOCR photograph of comet Kohoutek 1973f taken on 1974 January 14. Exposure was 8^m on IIa-O emulsion, centered on $1^h48^m37^s$ UT. Tick marks above the tail in this and succeeding photographs denote locations at which tail width measurements were made (Table 1), and the horizontal bars denote a distance of 10^6 km along the tail. (*b*) JOCR photograph of comet Kohoutek 1973f taken on 1974 January 17, $1^h40^m30^s$ UT (mid-exposure). Emulsion was IIa-O, exposure length was 10^m; a UG-1 filter was used. (*c*) JOCR photograph of comet Bradfield 1974b taken on 1974 March 23, $2^h55^m27^s$ UT (mid-exposure). Exposure length was 9^m15^s and emulsion was IIa-O. (*d*) JOCR photograph of comet Bradfield 1974b taken on 1974 April 9, centered on $1^h55^m45^s$ UT. The 15^m exposure was made on IIa-O emulsion.

ERSHKOVICH *et al.* (*see* page 398)